Scientific Reports

https://doi.org/10.1038/s41598-026-49748-w

Article in Press

Energy and thermal magnetization of diatomic molecules under the enhanced Pöschl-Teller potential

Received: 17 November 2025

Accepted: 16 April 2026

Published online: 25 April 2026

Cite this article as: Eyube E.S., Kamaludeen M., Vijinti F.C. *et al.* Energy and thermal magnetization of diatomic molecules under the enhanced Pöschl-Teller potential. *Sci Rep* (2026). https://doi.org/10.1038/s41598-026-49748-w

E. S. Eyube, M. Kamaludeen, F. C. Vijinti, I. I. Fwangle & M. F. Isa

Energy and thermal magnetization of diatomic molecules under the enhanced Pöschl-Teller potential

E. S. Eyube[1*a], M. Kamaludeen[1b], F. C. Vijinti[2c], I. I. Fwangle[3d], M. F. Isa[1e]

[1]Department of Physics, Faculty of Physical Sciences, Modibbo Adama University, P.M.B. 2076, Yola, Adamawa State, Nigeria.

[2]Department of Basic and Applied Science, College of Agriculture, Science and Technology, P.M.B. 1025, Jalingo, Taraba State, Nigeria

[3]Department of Physical Science Education, Faculty of Education, Modibbo Adama University, P.M.B. 2076, Yola, Adamawa State, Nigeria.

[*]Corresponding author: [a]Email: edwineyubes@mau.edu.ng: ORCID: 0000-0001-5059-0393

[b]Email: m.kamaludeen@mau.edu.ng: ORCID: 0009-0007-3380-9649

[c]Email: cosmas1044@gmail.com: ORCID ID: 0000-0001-8769-1526

[d]Email: m.scpse220851@student.mau.edu.ng: ORCID: 0009-0007-9995-6270

[e]Email: isafaisal@mau.edu.ng: ORCID: 0009-0005-0421-529X

Abstract: The Schrödinger equation is solved analytically for a particle subject to an enhanced Pöschl-Teller (EPT) potential in the presence of an external magnetic field and an Aharonov-Bohm flux field that induces topological phase effects. The bound state ro-vibrational energy equations are obtained using the generalized fractional Nikiforov-Uvarov method in conjunction with the Pekeris approximation scheme. The fractional order is introduced as an effective parameter that accounts for nonlocal and anharmonic ro-vibrational interactions that are not fully represented within the standard integer order framework. Based on these energy expressions, the mean thermal magnetization is derived within the partition function formalism. Numerical applications to diatomic molecules such as CO ($X\ ^1\Sigma^+$), Cs_2 ($3\ ^3\Sigma_g^+$), ICl ($X\ ^1\Sigma_g^+$), $^7Li_2$ ($1\ ^3\Delta_g$), Na_2 ($C(2)\ ^1\Pi_u$), and NaK ($c\ ^3\Sigma^+$) show that the mean percentage absolute deviation values decrease from 0.0990 %, 0.1407 %, 1.0027 %, 1.9504 %, 0.1234 %, and 0.9811 % to 0.0905 %, 0.1020 %, 0.5501 %, 1.1756 %, 0.0474 %, and 0.4840 % when fractional parameters are incorporated, indicating improved agreement with experimental data and enhanced flexibility of the ro-vibrational energy model. The analysis further shows that, at fixed temperatures, the mean thermal magnetization of the Na_2 ($C(2)\ ^1\Pi_u$) dimer increases with increasing magnetic field strength, highlighting the sensitivity of the system to external field variations. These results establish the EPT potential combined with a fractional order formulation as a reliable and adaptable analytical framework for describing the quantum and thermomagnetic behavior of diatomic molecules influenced by magnetic and topological quantum fields.

Keywords: Magnetization; Ro-vibrational energy; Partition function; Diatomic molecules; Schrödinger equation; Fractional parameters

1. Introduction

Thermodynamics is a fundamental aspect of physics with numerous applications in science and technology. It involves the study of how a system interacts with its surroundings. Key physical variables used to characterize thermodynamic processes include energy, entropy, heat capacity, and mean thermal energy, among others. Many physical systems, such as chemical reactors, heat pumps, and power plants, rely on thermodynamics for optimal operation. Thermodynamics has been applied to investigate phenomena such as heat conduction [1] and phase transitions [2], and to establish equilibrium constants in chemical reactions involving nitrogen and oxygen gases [3].

Magnetization and magnetic susceptibility are fundamental concepts in physical sciences and engineering. These concepts play a vital role in designing magnetic materials for electronics, augmenting energy storage through persistent currents in superconducting applications, and understanding biological systems in medical diagnostics. The magnetic separation technique, which relies on magnetization, has significantly improved biopharmaceutical protein purification in the drug industry [[4], [5]], and magnetic susceptibility measurements have been used to improve data collection efficiency for forensic research [6] and to assess heavy metal concentrations in soils [7].

There is increasing interest in applying analytical equations to investigate the physical properties of diatomic molecules. This approach relies on fewer spectroscopic constants of a diatomic molecule to analyze its physical properties and offers a more efficient alternative to experimental techniques, which involve substantial setup time and cost. Model equations derived for different diatomic oscillators have been used to explore thermal physical properties of diatomic molecules, such as Gibbs free energy, entropy, heat capacity, enthalpy, and index of refraction [[8], [9], [10], [11], [12]], as well as magnetic physical properties, including magnetization, magnetic susceptibility, and persistent current [[13], [14], [15], [16], [17], [18]].

The first step in constructing analytical models to study the physical properties of diatomic molecules requires solving a wave equation to obtain an algebraic description of the eigenenergies for the system. The time-independent Schrödinger wave equation (TISWE) has been solved for various exponential-type and hyperbolic-type diatomic oscillators. Some of the most commonly used methods for deriving analytical solutions to the TISWE and other equations of

mathematical physics include the exact quantization rules [[19], [20]], the SUSYQM method [21], the Laplace transform method [22], extended Nikiforov-Uvarov method [23], and the Feynman propagator method, the well-known path integral solution approach [[24], [25]]. These methods provide expressions for ro-vibrational energy levels in terms of the equilibrium bond distance (ρ_e), the rotational-vibrational coupling factor (α_e), the equilibrium harmonic vibrational frequency (ω_e), and the equilibrium dissociation energy (D_e). While these formulations accurately reproduce molecular spectra within the conventional integer-order framework, they are intrinsically local and may not fully capture residual anharmonicity, long-range correlations, or cumulative rovibrational coupling effects present in real diatomic molecules [26].

Fractional calculus has gained significant interest across various scientific and technological fields. This branch deals with non-integer order differentiation and integration, distinguishing it from traditional calculus [27]. Fractional calculus is particularly useful for modeling complex systems with memory and nonlocal effects, providing effective descriptions of behaviors such as anomalous diffusion and stress-strain relations in complex materials [28]. Additionally, fractional-order controllers enhance system performance and stability in dynamic applications, exemplifying the versatility of this mathematical framework in addressing real-world challenges [29].

In quantum and molecular systems, fractional-order formalisms are commonly interpreted as phenomenological extensions of standard theories, where the fractional order acts as an effective parameter that incorporates unresolved interactions and collective effects, rather than indicating a fundamental departure from quantum mechanics [[30], [31]].

Within this context, the generalized fractional derivative (GFD) approach introduces fractional parameters that enhance the flexibility of ro-vibrational energy expressions, allowing improved alignment with experimental data for diatomic molecules. The fractional order introduced in this framework does not imply that a diatomic molecule is fractional in a literal physical sense; instead, it serves as an effective descriptor that captures nonlocality, anharmonicity, and accumulated rovibrational interactions that are only approximately represented in integer-order models [[30], [32]].

This approach has led to accurate solutions for wave equations involving potential energy functions, including the improved Deng-Fan potential, improved Tietz potential, and improved Rosen-Morse potential [[33], [34], [35]]. It has also been used to determine bound-state energies and wave functions for other potentials, such as the Pseudoharmonic and Kratzer-Fues [36].

This study explores the enhanced Pöschl-Teller (EPT) potential, a specific form of the hyperbolic-type potential (HTP) used in various fields, including chemistry, atomic and molecular physics, and nuclear physics [37].

Previous research has applied improved versions of HTPs to solve the Schrödinger equation, enabling the description of energy levels in diatomic molecules. Equations derived from the EPT potential have proven effective in studying the energy states of several diatomic molecules, including SiF^{+} ($X\ ^{1}\Sigma^{+}$), O_2^{+} ($X\ ^{2}\Pi_g$), N_2^{+} ($X\ ^{1}\Sigma_g^{+}$), CO ($X\ ^{1}\Sigma^{+}$), ScI ($B\ ^{1}\Pi$), and RbH ($X\ ^{1}\Sigma^{+}$) [38]. Furthermore, approximate relativistic energy equations for a deformed hyperbolic barrier potential with a Coulomb-like tensor have been developed to analyze the energy levels of $^{7}Li_2$ ($G\ ^{1}\Pi_g$) and RbH ($X\ ^{1}\Sigma^{+}$) [39].

Additionally, thermodynamic models based on the EPT oscillator have been employed to investigate the thermal properties of the P_2 ($X\ ^{1}\Sigma_g^{+}$) dimer, including calculations of molar entropy, enthalpy, Gibbs free energy, and isobaric heat capacity [40], and equations for energy eigenvalues and thermodynamic properties have been derived to study the physical characteristics of RbH ($X\ ^{1}\Sigma^{+}$) molecules [[41], [42]].

Although conventional HTP energy expressions accurately predict molecular spectra, the absence of fractional parameters limits their adaptability when subtle nonlocal and anharmonic effects become significant. Incorporating fractional parameters through the GFD Schrödinger equation provides an effective means of refining the ro-vibrational energy structure and associated thermomagnetic properties, yielding a more comprehensive description of diatomic molecular behavior while remaining fully consistent with the established quantum-mechanical framework [[31], [32]]. The remainder of the paper is organized as follows: Section 2 derives the equation for the ro-vibrational energy levels; Section 3 derives the magnetic functions; Section 4 presents the results and discussion; and Section 5 provides a brief conclusion.

2. The equation for ro-vibrational energy levels of the EPT oscillator

The Pöschl-Teller potential was first introduced by Pöschl and Teller in 1933 in its hyperbolic form, establishing a solvable class of hyperbolic-type potentials in quantum mechanics. It is defined as [37]

$$U_{PT}(r) = \frac{U_1}{\sinh^2 a(r - r_0)} + \frac{U_2}{\cosh^2 a(r - r_0)},$$

(1)

Here, α is related to the range of the potential, ρ is the bond distance, ρ_0 is a real constant, and U_1 and U_2 are the potential strengths.

The coordinate shift $r \to r - r_0$ is an intrinsic feature of the original Pöschl-Teller potential formulation [37], where ρ_0 specifies the equilibrium position of the interaction, and therefore does not constitute an additional transformation introduced in the present work. This model was originally proposed to describe short-range interactions using hyperbolic functions. While mathematically solvable, the original Pöschl-Teller potential cannot be applied directly to diatomic molecules in its current form.

The present model, called the enhanced Pöschl-Teller (EPT) potential, is a generalized form built from the same family of hyperbolic functions (sinh(x), cosh(x)) and is expressed as

$$U(r) = U_0 + \frac{U_1 - U_2 \cosh a(r - r_0)}{\sinh^2 a(r - r_0)},$$

(2)

It is called enhanced because it adds an independent parameter, U_0, which allows control over potential depth, range, and asymmetry. The constant U_0 fixes the reference energy by enforcing the condition $U(\rho_e) = 0$ and does not alter the shape of the interaction potential or any physical observables, as demonstrated in Appendix B This extension preserves the solvable hyperbolic structure of the original potential while making it suitable for modeling diatomic molecular systems.

The Morse potential is widely used to describe diatomic molecules and successfully accounts for anharmonicity and bond dissociation [43]. It provides a simple analytical expression for the potential energy curve and allows straightforward calculation of vibrational energy levels. However, its functional form prescribes a fixed shape once the molecular constants are set, which can

limit accuracy for higher vibrational and ro-vibrational states and reduce flexibility in modeling subtle variations in the bond potential [44].

In contrast, the EPT potential, constructed from hyperbolic functions and defined by the parameters U_0, U_1, U_2, α, and q, allows independent control of the depth, range, and asymmetry of the interaction potential. This flexibility enables it to capture both short-range repulsion and intermediate-range attraction, particularly when combined with fractional parameters [27], making the EPT a physically motivated and adaptable alternative to the Morse potential for modeling diatomic molecular interactions.

To achieve the objectives of the study, it is necessary to solve the TISWE for a system constrained within a 2D electromagnetic potential field. For such a system, the TISWE is given by [[18], [45]]

$$H\varphi_{nm}(r)=E_{nm}\varphi_{nm}(r),$$

(3)

where $\varphi_{nm}(\rho)$ is the radial wave function, E_{nm} is the eigen energy, n is the vibrational quantum number (n = 0, 1, 2, ...), and m is the magnetic quantum number (m = 0, ±1, ±2, ...). The Hamiltonian operator H of the system is expressed as

$$H=-\frac{\hbar^2}{2\mu}\frac{d^2}{dr^2}+U(r)+\frac{2B^2e^2}{a^2\mu c^2}\tanh^2\tfrac{1}{2}ar$$
$$+\frac{\hbar Be}{a\mu c}\left(m+\frac{\Phi_{AB}}{\hbar\pi c}\coth\tfrac{1}{2}ar\right)+\frac{\hbar^2}{8\mu r^2}\left(m+\frac{\Phi_{AB}}{\pi\hbar c}\right)^2+3m^2-1\Big]$$

(4)

where $\hbar$ is the reduced Planck constant, μ is the effective mass of the system, e is the electronic charge, c is the speed of light, B (Tm^{-1}) is the uniform magnetic field, and Λ_{AB} (Tm) represents the Aharonov-Bohm flux introduced via the vector potential $\mathbf{A}=\left(Br+\Phi_{AB}/2\pi r\right)\hat{\boldsymbol{\varphi}}$ following Ref. [18], which includes both the uniform magnetic field and the AB flux contributions, producing the corresponding flux-dependent phase shift in the wavefunction. The TISWE is reformulated by inserting expressions (4) and (2) into (3) to yield

$$\frac{d^2f_{nm}(r)}{dr^2}+\frac{2\mu}{\hbar^2}\left[E_{nm}-U_0-\frac{U_1-U_2\cosh a(r-r_0)}{\sinh^2 a(r-r_0)}-\frac{2B^2e^2\tanh^2\left(\frac{1}{2}ar\right)}{a^2\mu c^2}-\frac{\hbar^2 l}{2\mu r_e^2}\left(-\frac{\hbar Bek}{a\mu c r_e}\right)\right]f_{nm}(r)=0.$$

(5)

In this equation, $k = m + \epsilon_{AB}/\hbar c$, $l = \frac{1}{4}\left(k^2 + 3m^2 - 1\right)$, $f = r_e^2/r^2$, and $g = \frac{r_e}{r}\tanh\left(\frac{1}{2}ar\right)$.

To obtain an analytically solvable differential equation, the dimensionless functions f_{exact} and g_{exact} are represented by the following Pekeris approximations [[46], [47]]

$$f \approx f_{appr} = l_0 + \frac{l_1 + l_2\cosh a\left(r - r_0\right)}{\sinh^2 a\left(r - r_0\right)}, \tag{6}$$

$$g \approx g_{appr} = k_0 + \frac{k_1 + k_2\cosh a\left(r - r_0\right)}{\sinh^2 a\left(r - r_0\right)}, \tag{7}$$

where κ_k, λ_k ($k = 0, 1, 2$) are expansion coefficients whose development is given in Appendix A.

The function $\tanh^2\left(\frac{1}{2}ar\right)$ can be approximated by $\tanh^2\frac{1}{2}a\left(r - r_0\right)$, which is valid for small values of ρ and ρ_0 of the order of ρ_e. Using this approximation along with expressions (6) and (7), equation (5) can be rewritten as follows

$$\psi''_{nm}(s) + \frac{\frac{1}{2}(1 - 3s)}{s(1 - s)}\psi'_{nm}(s) + \frac{-\sigma_1 s^2 + \sigma_2 s - \sigma_3}{s^2(1 - s)^2}\psi_{nm}(s) = 0, \tag{8}$$

where

$$\sigma_1 = \frac{2m}{a^2\hbar^2}\left[\frac{1}{4}\left(U_1 + U_2\right) + \frac{\hbar B_e k}{4amcr_e}\left(k_1 - k_2\right) + \frac{\hbar^2 l}{8mr_e^2}\left(l_1 - l_2\right) + \frac{2B_e^2 e^2}{a^2 mc^2}\right], \tag{9a}$$

$$\sigma_2 = \frac{2m}{a^2\hbar^2}\left[E_{nm} - U_0 + \frac{U_1}{2} - \frac{\hbar B_e k}{2amcr_e}\left(2k_0 - k_1\right) - \frac{\hbar^2 l}{4mr_e^2}\left(2l_0 - l_1\right)\right], \tag{9b}$$

$$\sigma_3 = \frac{2m}{a^2\hbar^2}\left[\frac{1}{4}\left(U_1 - U_2\right) + \frac{\hbar B_e k}{4amcr_e}\left(k_1 + k_2\right) + \frac{\hbar^2 l}{8mr_e^2}\left(l_1 + l_2\right)\right], \tag{9c}$$

prime stands for differentiation with respect to ρ, and $s = \tanh^2\frac{1}{2}a\left(r - r_0\right)$.

In the integer-order limit of the formalism, the present EPT model reduces to the improved generalized Pöschl-Teller potential reported in Ref. [48], and the

recovery of identical integer-order results serves as a consistency check, while the novelty of the present work resides in the generalized fractional extension.

At this stage, equation (8) can be solved using standard techniques like the parametric Nikiforov-Uvarov method which have proven to be successful for solving wave and other useful equations of mathematical physics [49]. However, this work employs the more precise generalized fractional Nikiforov-Uvarov (GFNU) formalism. A brief overview of the GFNU method is provided below, but a complete description of the methodology is available in publication [36]. In the GFNU formalism, the fractional derivative of a function $\varphi(z)$ is given as

$$D\varphi(z)=\lim_{d\to 0}\frac{\varphi\left(z+bd(z)^{1-a}\right)-\varphi(z)}{d},$$

(10)

where $b=\frac{\Gamma(C)}{\Gamma(C-a+1)}$, Δ is a generalized fractional differential operator. a and C are fractional parameters satisfying $0 < a \leq 1$, $C \in R^{+}$, and $\Gamma(x)$ denotes the standard gamma function evaluated at x [36]. The operator Δ has the property that

$$D^{a}\{\varphi(z)\}=bz^{1-a}\varphi'(z).$$

(11a)

$$D^{a}\{D^{a}\varphi(z)\}=b^{2}\{z^{2(1-a)}\varphi''(z)+(1-a)z^{1-2a}\varphi'(z)\}.$$

(11b)

Given a hypergeometric-type differential equation of the form

$$y''_{nm}(s)+\frac{a_1-a_2s}{s(1-a_3s)}y'_{nm}(s)+\frac{-b_1s^2+b_2s-b_3}{s^2(1-a_3s)^2}y_{nm}(s)=0,$$

(12)

the GFNU method replaces integer with fractional derivatives, this approach transforms expression (12) to the following form [36]

$$D^{a}\left(D^{a}y_{nmab}(s)\right)+\frac{a_1-a_2s^{a}}{s^{a}(1-a_3s^{a})}D^{a}y_{nmab}(s)+\frac{-b_1s^{2a}+b_2s^{a}-b_3}{s^{2a}(1-a_3s^{a})^{2}}y_{nmab}(s)=0.$$

(13)

The condition leading to polynomial solution of (13) is given as

$$n^2a^2b^2a_3+nab(a_2-a_3ab)-ab(2n+1)a_5+ab(2n+1)\left(\sqrt{a_9}+a_3\sqrt{a_8}\right)+a_7+2a_3a_8+2\sqrt{a_8a_9}=0,$$

(14)

where

$$a_4=\tfrac{1}{2}(ab-a_1),\quad a_5=\tfrac{1}{2}(a_2-2a_3ab)$$
$$a_6=a_5^2+b_1,\quad a_7=2a_4a_5-b_2, a_8=a_4^2+b_3.$$
$$a_9=a_3a_7+a_3^2a_8+a_6$$

(15)

To execute the GFNU formalism in (8), the integer order derivatives are replaced with fractional order derivatives to yield

$$D^a\left[D^aj_{nmab}(s)\right]+\frac{\frac{1}{2}\left(1-3s^a\right)}{s^a\left(1-s^a\right)}D^aj_{nmab}(s)+\frac{-c_1s^{2a}+c_2s^a-c_3}{s^{2a}\left(1-s^a\right)^2}j_{nmab}(s)=0.$$

(16)

Evidently, equation (13) is comparable to (16) provided $a_1=\frac{1}{2}$, $a_2=\frac{3}{2}$, $a_3=1$; $b_1=c_1$, $b_2=c_2$, $b_3=c_3$. These results inserted into (15) gives $a_4=\frac{1}{2}ab-\frac{1}{4}$, $a_5=-ab+\frac{3}{4}$, $a_6=a_5^2+c_1$, $a_7=2a_4a_5-c_2$, $a_8=a_4^2+c_3$, and $a_9=\frac{1}{4}(ab-1)^2+c_1-c_2+c_3$. These values are used in (14), the resulting expression is simplified to deduce

$$c_2=c_1+c_3+\frac{1}{4}(ab-1)^2-\left[ab\eta+\frac{1}{2}\sqrt{\left(\frac{1}{2}ab-\frac{3}{4}\right)^2+c_1}+\sqrt{\left(\frac{1}{2}ab-\frac{1}{4}\right)^2+c_3}\right]^2.$$

(17)

The expressions in (9a), (9b), and (9c) are used to substitute for c_1, c_2, and c_3 in (17), this leads to

$$E_{nm}\to E_{nmab}=U_0+\frac{\hbar Bekk_0}{amcr_e}+\frac{\hbar^2/I_0}{2mr_e^2}+\frac{2B^2e^2}{a^2mc^2}+\frac{a^2\hbar^2(ab-1)^2}{8m}-\frac{a^2\hbar^2}{2m},$$
$$\left[ab\eta+\frac{1}{2}\sqrt{\left(\frac{1}{2}ab-\frac{3}{4}\right)^2+\frac{2m}{a^2\hbar^2}(U_1+U_2)+\frac{2Bek}{a^3\hbar cr_e}(k_1-k_2)+\frac{I}{a^2r_e^2}(I_1-I_2)+\frac{4B^2e^2}{a^4\hbar^2c^2}}\right.$$
$$\left.+\sqrt{\left(\frac{1}{2}ab-\frac{1}{4}\right)^2+\frac{2m}{a^2\hbar^2}(U_1-U_2)+\frac{2Bek}{a^3\hbar cr_e}(k_1+k_2)+\frac{I}{a^2r_e^2}(I_1+I_2)}\right]^2.$$

(18)

The GFNU method offers flexibility by allowing for adjustments to the fractional parameters, which enables the formulation of ordinary derivative equations. By

setting $a = C = 1$, it follows that b must be 1. Therefore, the ordinary derivative formulation for equation (18) is as follows

$$E_{nm} = U_0 + \frac{\hbar B e k k_0}{a\pi m c r_e} + \frac{\hbar^2 I / I_0}{2 m r_e^2} + \frac{2 B^2 e^2}{a^2 m c^2} - \frac{a^2 \hbar^2}{2m},$$
$$\left\{ n + \frac{1}{2} - \sqrt{\frac{1}{16} + \frac{2m}{a^2\hbar^2}(U_1 + U_2) + \frac{2Bek}{a^3 \hbar c r_e}(k_1 - k_2) + \frac{I}{a^2 r_e^2}(I_1 - I_2) + \frac{4B^2 e^2}{a^4 \hbar^2 c^2}} \right\}^2 \cdot$$
$$+ \sqrt{\frac{1}{16} + \frac{2m}{a^2\hbar^2}(U_1 - U_2) + \frac{2Bek}{a^3 \hbar c r_e}(k_1 + k_2) + \frac{I}{a^2 r_e^2}(I_1 + I_2)}$$

(19)

3. The Mean Thermal Magnetization Function

In this section, the mean thermal magnetization model for the EPT potential is derived. A key component in obtaining this function is the internal partition function given as [50]

$$Z = \sum_{l=0}^{\infty} \sum_{n=0}^{\infty} (2l+1) \exp(-\beta E_{nmab}),$$

(20)

where, $\Box = |m|$ is the rotational quantum number, $\beta^{-1} = k_B T$, where T is the absolute temperature and k_B is the Boltzmann coefficient. By restricting the system to pure vibrational motion, $\Box = 0$. For this setting, the partition function is rewritten

$$Z = e^{-t^2} \sum_{n=0}^{N_{max}} z(n), \quad z(n) = e^{u^2 (n - N_{max})^2}, \quad u = a\hbar ab \sqrt{\frac{b}{2m}}$$
$$t = \sqrt{b \left[U_0 + \frac{Be^2 k_0 L_{AB}}{a\pi m c^2 r_e} + \frac{\hbar^2 I / I_0}{2 m r_e^2} + \frac{2B^2 e^2}{a^2 m c^2} + \frac{a^2 \hbar^2 (ab-1)^2}{8m} \right]},$$

(21)

The upper limit of the summation in (21), also referred to as the number of excited bonded states is evaluated from the expression $\left. \frac{\partial E_{n0ab}}{\partial n} \right|_{N_{max}} = 0$ to obtain $N_{max} = X - Y$, where

$$X = -\frac{1}{2} + \sqrt{\left(\frac{1}{2} - \frac{3}{4ab} \right)^2 + \frac{2m(U_1 + U_2)}{a^2 \hbar^2 a^2 b^2} + \frac{I_1 - I_2}{a^2 a^2 b^2 r_e^2} \left(\frac{L_{AB}}{\pi \hbar c} \right)^2 - 1} + \frac{4B^2 e^2}{a^4 \hbar^2 a^2 b^2 c^2} + \frac{2Be^2 L_{AB}(k_1 - k_2)}{a^3 \pi \hbar^2 a^2 b^2 c^2 r_e},$$

(22a)

$$Y=\sqrt{\left(\frac{1}{2}-\frac{1}{4ab}\right)^2+\frac{2m(U_1-U_2)}{a^2h^2a^2b^2}+\frac{I_1+I_2}{a^2a^2b^2r_e^2}\left[\left(\frac{L_{AB}}{\pi hc}\right)^2-1\right]+\frac{2Be^2L_{AB}(k_1+k_2)}{a^3\pi h^2a^2b^2c^2r_e}}.$$

(22b)

The function $\zeta(n)$ does not allow for the exact evaluation of the summation in (21). However, a quasi-exact expression for the partition function can be derived using the following expression [45]

$$\sum_{n=0}^{N_{max}} z(n)\approx\frac{1}{2}\{z(0)-z(N_{max}+1)\}+\int_0^{N_{max}+1} z(n)\,dn.$$

(23)

By using equation (23) and the expression for $\zeta(n)$, the approximate form of the internal partition function is deduced as follows

$$Z=\frac{1}{2}\left(e^{u^2N_{max}^2-t^2}-e^{u^2-t^2}\right)+\frac{\sqrt{\pi}}{2u}e^{-t^2}\left(\mathrm{Erfi}\,uN_{max}-\mathrm{Erfi}\,u\right),$$

(24)

in this context, Erfi(y) denotes the imaginary error function of the parameter y. The mean thermal magnetization (M) is given as [51]

$$M=\frac{1}{b}\frac{\partial}{\partial B}\ln Z.$$

(25)

For completeness, the derivatives needed for (25) is deduced from equations (24), and (21) as

$$\frac{\partial\ln Z}{\partial B}=-2t\frac{\partial t}{\partial B}+\frac{u^2N_{max}+1}{Z}\left(\frac{\partial X}{\partial B}-\frac{\partial Y}{\partial B}\right)e^{u^2N_{max}^2-t^2}.$$

(26)

$$t\frac{\partial t}{\partial B}=\frac{be^2}{am\pi^2}\left(\frac{k_0L_{AB}}{2\pi^2}+\frac{2B}{a}\right),$$

(27a)

$$\frac{\partial X}{\partial B}=\frac{2e^2}{a^3h^2a^2b^2c^2}\frac{1}{2X+1}\left[\frac{4B}{a}+\frac{L_{AB}(k_1-k_2)}{\pi}\right],$$

(27b)

$$\frac{\partial Y}{\partial B} = \frac{2e^2 L_{AB}(k_1 + k_2)}{a^3 \pi \hbar^2 a^2 b^2 c^2 Y}.$$

(27c)

Equations (25), (26), (27a), (27b), and (27c) are combined to yield the explicit equation for the mean thermal magnetization in the form

$$M = -\frac{e^2}{am c^2}\left(\frac{k_0 L_{AB}}{\pi^2} + \frac{4B}{a}\right) + \frac{2e^2\left(u^2 N_{max} + 1\right)}{a^3 b \hbar^2 a^2 b^2 c^2 Z}\left(\frac{1}{2X+1}\frac{4B}{a} + \frac{L_{AB}}{\pi}\left(\frac{k_1 - k_2}{2X+1} - \frac{k_1 + k_2}{Y}\right)\right) e^{u^2 N_{max}^2 - t^2}.$$

(28)

4. Results and Discussion

This section applies the derived equations to selected diatomic molecules, namely CO ($X\ ^1\Sigma^+$), Cs_2 ($3\ ^3\Sigma_g^+$), ICl ($X\ ^1\Sigma_g^+$), $^7Li_2$ ($1\ ^3\Delta_g$), Na_2 ($C(2)\ ^1\Pi_u$), and NaK ($c\ ^3\Sigma^+$). These systems are representative of molecules that are experimentally accessible and theoretically well studied, making them suitable for validating the proposed model.

Carbon monoxide, CO ($X\ ^1\Sigma^+$), plays an important role in interstellar chemistry by acting as a primary ice component on which complex organic molecules form in prestellar environments, thereby influencing chemical evolution in cold astronomical regions [52]. Cesium dimer, Cs_2 ($3\ ^3\Sigma_g^+$), together with other alkali dimers, serves as a central system in cold and ultracold molecule research, where controlled association and manipulation of molecular states enable investigations of quantum many body dynamics and precision measurements at ultralow temperatures [53]. The heteronuclear interhalogen molecule ICl ($X\ ^1\Sigma_g^+$) is widely employed in electron collision and scattering studies that provide insight into atmospheric processes and molecular collision dynamics, offering valuable benchmarks for theoretical descriptions of low energy interactions [54].

The light alkali dimer $^7Li_2$ ($1\ ^3\Delta_g$) is commonly used in cold and ultracold molecule studies as a prototypical diatomic system for testing quantum control techniques, precision spectroscopy, and fundamental collision dynamics at microkelvin temperatures [53]. Sodium dimer Na_2 ($C(2)\ ^1\Pi_u$) functions as a model system in precision molecular spectroscopy and quantum control experiments, where excited electronic state dynamics and collisional processes can be examined with high resolution [53]. The mixed alkali molecule NaK ($c\ ^3\Sigma^+$) is particularly relevant to the creation of ultracold polar molecular gases

with strong electric dipole moments, which support studies of quantum simulation, dipolar interactions, and quantum many body phenomena [55].

These molecules possess well characterized molecular constants, including the equilibrium bond distance (ρ_e), the rotational vibrational coupling factor (α_e), the harmonic vibrational frequency (ω_e), and the dissociation energy (D_e). These parameters serve as input data for the model equations. The experimental values for these constants are obtained from Refs. [[56], [57], [58], [59], [60], [61]]. Table 1 summarizes these constants.

For the model equations to be applicable to diatomic systems, the Varshni conditions for a diatomic oscillator must be satisfied, as given in Ref. [62]

$$\lim_{r\to\infty} U(r) - U(r_e) = D_e, \tag{29a}$$

$$U'(r_e) = 0, \tag{29b}$$

$$U''(r_e) = k_e, \tag{29c}$$

$$a_e = -\left[1 + \frac{r_e}{3}\frac{U'''(r_e)}{U''(r_e)}\right]\sqrt{\frac{6B_e^2}{\omega_e}}, \tag{29d}$$

where $B_e = \hbar/4\pi c\mu r_e^2$ is the equilibrium rotational constant, k_e and α_e are the equilibrium bond stiffness and rotation-vibration interaction constant, respectively. Formulation of the potential parameters of the EPT oscillator are detailed in Appendix B.

4.1. Bound-state energies of the diatomic molecules

This section analyzes the bound-state energy eigenvalues of the EPT potential with the electromagnetic field disabled, enabling direct comparison between predicted energy eigenvalues and experimental results. Setting both B and Λ_{AB} to zero in equation (5) yields $l = m' - \frac{1}{4}$, indicating that the term $\left(\hbar^2/2\mu r_e^2\right)l$ in the TISWE remains non-vanishing regardless of the magnetic quantum number m. Consequently, the ro-vibrational energies predicted by equation (18) depend

strongly on the agreement between the exact function f and the approximate form f_{appr}, as applied in approximation (6).

Figure 1 shows a comparison of f and f_{appr} for CO ($X\ ^1\Sigma^+$), as defined in expression (6). The results show excellent agreement for bond distances near the equilibrium internuclear separation. Figure 2 presents the same comparison for Cs_2 ($3\ ^3\Sigma_g^+$), which also exhibits strong agreement near the equilibrium region. These results confirm that the Pekeris approximation is reliable across different diatomic systems. Additional figures for ICl ($X\ ^1\Sigma_g^+$), $^7Li_2$ ($1\ ^3\Delta_g$), Na_2 ($C(2)\ ^1\Pi_u$), and NaK ($c\ ^3\Sigma^+$) are not shown, as their approximation curves follow the same trends observed for CO and Cs_2. The similarity across molecular systems supports the broad applicability of the approximation scheme for solving the TISWE.

Equation (5) further shows that when the magnetic and AB fields are simultaneously activated ($B \neq 0$, $\Lambda_{AB} \neq 0$), the term $(\hbar B e k / a m c r_e)g$ becomes nonzero. While physically relevant, this term does not yield a closed-form analytical expression for the ro-vibrational energy spectrum. To restore analytical solvability, the approximation function g_{appr}, defined in expression (7), is introduced as a substitute for the exact function g.

Figure 3 shows a comparison of g and g_{appr} for CO ($X\ ^1\Sigma^+$), while Figure 4 shows the same comparison for Cs_2 ($3\ ^3\Sigma_g^+$). In both cases, the approximation reproduces the exact function accurately for ρ values near the equilibrium separation ρ_e, confirming that it provides an analytical solution to the TISWE even when both fields are active. Plots for the remaining molecules show nearly identical equilibrium-region behavior, with overlapping curve profiles and no additional qualitative deviations. This consistency explains the omission of separate figures for those molecules, since repeating similar plots would provide no new physical or analytical insight. The approximation performance remains uniform across all molecular systems analyzed.

Using equation (18), energy eigenvalues are computed by tuning the fractional parameters a and C to reproduce observed spectral data, including Rydberg-Klein-Rees (RKR) results reported in [[57], [58], [59], [60], [61], [63]]. For reference, equation (19) is also evaluated with the fractional parameters set to one, corresponding to the deactivated case.

The calculation of ro-vibrational energies for the case $B \neq 0$ and $\Lambda_{AB} \neq 0$ is not included, since no experimental data are available for comparison. The Pekeris approximation remains applicable under these conditions. The resulting energy eigenvalues for all molecules, with the electromagnetic field disabled ($B = 0$, $\Lambda_{AB} = 0$), are summarized in Tables 2-4.

To quantify agreement with experimental data, the percentage absolute deviation (PAD) is computed using expression $\mathrm{PAD} = 100\left(1 - E_{\mathrm{pred}}/E_{\mathrm{obs}}\right)$, where $E_{\mathrm{pred}} \equiv (E_{nmab}, E_{nm})$ and E_{obs} represents experimental energies reported in Refs. [[64], [65]]. This measure provides a direct numerical comparison between predicted and observed vibrational energy levels, allowing evaluation of model accuracy against reference spectroscopic results.

The Lippincott criteria is a standard condition in diatomic molecular spectroscopy requiring that predicted vibrational energy levels maintain a mean percentage absolute deviation below 1% when compared with experimental spectra [[48], [66]]. In this work, this condition is used to evaluate results from both Eqs. (18) and (19), ensuring that the activated and deactivated fractional parameter cases remain within validated deviation limits.

Consistent with the Lippincott condition, the mean PAD (MPAD) of predicted energy levels should remain below 1% of the experimental values. The MPAD values for each molecule are reported in Table 5, alongside values from alternative models, including the Modified Hyperbolic-Type (MHT) oscillator, Improved Generalized Pöschl-Teller (IGPT) oscillator, Morse (MOR) oscillator, Improved Scarf (IS) oscillator, Improved Tietz (IT) oscillator, Improved Rosen-Morse (IRM) oscillator, Improved Manning-Rosen (IMR) oscillator, Deformed Scarf (DS) oscillator, Specialized Pöschl-Teller (SPT) oscillator, and Deformed Pöschl-Teller (DPT) oscillator, as reported in Refs. [[34], [38], [49], [66], [67], [68], [69], [70], [71], [72]].

The results show that enabling fractional parameters substantially improves agreement with experimental spectra. The MPAD values obtained with fractional parameters are 0.0905% for CO, 0.1020% for Cs_2, 0.5501% for ICl, 1.1756% for $^7Li_2$, 0.0474% for Na_2, and 0.4840% for NaK. Without fractional parameters, the MPAD values increase to 0.0990%, 0.1407%, 1.0027%, 1.9504%, 0.1234%, and 0.9811%, respectively. These results confirm that incorporating fractional

parameters significantly enhances agreement with experimental spectra and improves predictive accuracy of the EPT oscillator relative to experimental data.

Overall, the EPT oscillator remains consistent with the Lippincott criteria for most molecules analyzed and produces MPAD values lower than many competing analytical models. Although the IT oscillator achieves better accuracy for the $^{7}Li_2$ dimer, both the IT and fractional EPT models remain within acceptable deviation limits. The consistently reduced MPAD values confirm that the EPT oscillator, particularly with fractional parameters enabled, provides a robust and broadly applicable analytical framework for predicting molecular energy spectra.

4.2. Application of the mean thermal magnetization to the Na_2 (C(2) $^{1}\Pi_u$) dimer

The magnetization of diatomic molecules can be analyzed using equation (28), with the Λ_{AB} field intensity set to 10^{-5} T Å, providing a general framework to compute their magnetic response under an external field. For illustrative purposes, the focus here is on the Na_2 (C(2) $^{1}\Pi_u$) dimer. Figure 5 shows the variation of its magnetization as a function of temperature for three magnetic field strengths (B = 50, 60, 70 T m^{-1}). The magnetization decreases monotonically with increasing temperature, reflecting the effect of thermal agitation opposing the alignment of molecular magnetic moments with the applied field. At low temperatures (~300 K), the magnetization reaches its maximum for each field: 6.41 × 10^{-46} Wb at B = 50 T m^{-1}, 7.69 × 10^{-46} Wb at B = 60 T m^{-1}, and 8.97 × 10^{-46} Wb at B = 70 T m^{-1}.

Increasing the magnetic field strength results in higher magnetization at any given temperature. For example, at 1000 K, magnetization rises from ~2.61 × 10^{-46} Wb at B = 50 T m^{-1} to ~3.04 × 10^{-46} Wb at B = 70 T m^{-1}. The temperature dependence is most pronounced at lower temperatures, while at higher temperatures the decrease in magnetization slows due to thermal randomization of magnetic moments.

Although the discussion focuses on Na_2 for clarity, equation (28) is equally applicable to the other diatomic molecules considered in this study, and similar qualitative trends are expected for all of them. This approach provides a general framework for examining molecular magnetization under external fields while keeping the presentation clear and concise.

5. Conclusions

This study formulates and solves the time independent Schrödinger equation for a system coupled with magnetic and Aharonov-Bohm flux fields within the enhanced Pöschl-Teller (EPT) oscillator framework. Using the generalized fractional Nikiforov-Uvarov method together with the Pekeris approximation, explicit expressions for the bound state ro-vibrational energy spectrum incorporating fractional parameters are obtained. The fractional formulation modifies the quantization condition governing the ro-vibrational energy eigenvalues while preserving the functional form of the EPT potential, introducing additional degrees of freedom at the level of the energy spectrum rather than through a reshaping of the interaction potential. An analytical expression for the mean thermal magnetization is derived from the fractional ro-vibrational energy levels and the corresponding partition function. Numerical calculations are performed for several diatomic molecules, namely CO ($X\ ^1\Sigma^+$), Cs_2 ($3\ ^3\Sigma_g^+$), ICl ($X\ ^1\Sigma_g^+$), $^7Li_2$ ($1\ ^3\Delta_g$), Na_2 ($C(2)\ ^1\Pi_u$), and NaK ($c\ ^3\Sigma^+$). Comparison with experimental Rydberg-Klein-Rees data using the mean percentage absolute deviation (MPAD) shows that when the fractional parameters are deactivated, the MPAD values are 0.0990 %, 0.1407 %, 1.0027 %, 1.9504 %, 0.1234 %, and 0.9811 %, respectively. When the fractional parameters are activated, these values improve to 0.0905 %, 0.1020 %, 0.5501 %, 1.1756 %, 0.0474 %, and 0.4840 %. This improvement arises from the increased flexibility of the ro-vibrational energy eigenvalues, which allows residual discrepancies associated with analytical approximations near the equilibrium internuclear separation to be effectively absorbed at the spectral level. Consequently, improved agreement between theoretical predictions and experimental energy spectra is achieved without altering the underlying potential model. The results further show that at fixed temperatures, the mean thermal magnetization of the Na_2 ($C(2)\ ^1\Pi_u$) dimer increases with magnetic field strength, indicating possible applications in molecular magnetism and field dependent thermodynamic systems. Consequently, the present framework demonstrates that fractional calculus is applied to the solution of the Schrödinger equation with the EPT potential, providing a reliable and adaptable analytical approach for modeling molecular systems influenced by magnetic and topological quantum fields**.** Future investigations may extend this formulation to more complex molecular geometries or alternative electromagnetic field configurations.

Statements and declarations

Funding: Not applicable

Conflict of interest/competing interest: We have no known competing financial interest or personal relationships that could have appeared to influence the work reported in this paper

Data availability statement: Data included in article/referenced in article

Code availability: Not applicable

Author contribution statement:

E. S. Eyube: Conceptualization, Supervision, Data curation, Writing-Original draft, Writing-Review and editing, Methodology, Validation, Formal analysis, Resource**.** Software. **M. Kamaludeen**: Validation, Writing-Original draft, Writing-Review and editing, Methodology, Software, Data curation **F. C. Vijinti**: Validation, Writing-Original draft, Writing-Review and editing, Methodology, Software, Data curation. **I. I. Fwangle**: Data curation, Writing-Original draft, Writing-Review and editing, Methodology, Formal analysis, Resource**.** Software. **M. Faisal**: Writing-Original draft, Writing-Review and editing, Methodology, Data curation, Formal analysis, Investigation, Validation, Visualization.

Ethics approval: Not applicable

Consent to participate: Not applicable

Consent for publication: Not applicable

Final version of the manuscript: All authors approved the final version of the manuscript submitted

Appendix A

This appendix presents the derivation of the expansion coefficients κ_k and λ_k for $k = 0, 1, 2$. For brevity, approximations (6) and (7) are restated in the compact form

$$f \approx \lambda_0 + \lambda_1 u + \lambda_2 v, \tag{A1}$$

$$g \approx k_0 + k_1 u + k_2 v, \tag{A2}$$

where the associated definitions are

$$f = \frac{r_e^2}{r^2}, \tag{A3}$$

$$g = \frac{r_e}{r}\tanh\left(\tfrac{1}{2}\alpha r\right), \tag{A4}$$

$$u = \operatorname{csch}^2\alpha(r - r_0), \tag{A5}$$

$$v = \operatorname{csch}^2\alpha(r - r_0)\cosh\alpha(r - r_0). \tag{A6}$$

The objective is to expand the functions $f(\rho)$, $g(\rho)$, $u(\rho)$, and $v(\rho)$ in a Taylor series around the equilibrium point $\rho = \rho_e$, giving

$$f \approx f_e + f_e'(r - r_e) + \frac{1}{2}f_e''(r - r_e)^2 + \cdots, \tag{A7}$$

$$g \approx g_e + g_e'(r - r_e) + \frac{1}{2}g_e''(r - r_e)^2 + \cdots, \tag{A8}$$

$$u \approx u_e + u_e'(r - r_e) + \frac{1}{2}u_e''(r - r_e)^2 + \cdots, \tag{A9}$$

$$v \approx v_e + v_e'(r - r_e) + \frac{1}{2} v_e''(r - r_e)^2 + \ldots .$$

(A10)

Here, a prime denotes differentiation with respect to ρ. The symbols f_e, ..., etc., represent the values of the corresponding functions evaluated at $\rho = \rho_e$. Using (A3) -(A6), the following expressions are obtained

$$f_e = 1, \quad f_e' = -\frac{2}{r_e}, \quad f_e'' = \frac{6}{r_e^2},$$

(A11)

$$g_e = \tanh\left(\tfrac{1}{2}\rho\right), \; g_e' = g_e\left(a \operatorname{sech}\rho - \frac{1}{r_e}\right), \; g_e'' = g_e\left(\frac{1}{2}a^2 \tanh^2\left(\tfrac{1}{2}\rho\right) - \frac{2a}{r_e}\operatorname{csch}\rho + \frac{2}{r_e^2}\right),$$

(A12)

$$u_e = \operatorname{csch}^2 q, \quad u_e' = -2a u_e \coth q, \quad u_e'' = 2a^2 u_e\left(2\coth^2 q + \operatorname{csch}^2 q\right),$$

(A13)

$$v_e = \operatorname{csch}^2 q \cosh q, \quad v_e' = -a v_e\left(2\coth q - \tanh q\right), \quad v_e'' = a^2 v_e\left(\coth^2 q + 5\operatorname{csch}^2 q\right),$$

(A14)

where $p = a r_e$, and $q = a\left(r_e - r_0\right)$. The auxiliary quantities $p = a r_e$, and $q = a\left(r_e - r_0\right)$ are introduced for notational simplicity. Substituting expansions (A7), (A9), and (A10) into (A1), and equating coefficients of $\left(r_e - r_0\right)^0$, $\left(r_e - r_0\right)^1$, and $\left(r_e - r_0\right)^2$, results in the linear system

$$l_0 + u_e l_1 + v_e l_2 = f_e.$$

(A15)

$$u_e' l_1 + v_e' l_2 = f_e'.$$

(A16)

$$u_e'' l_1 + v_e'' l_2 = f_e''.$$

(A17)

Solving (A15) -(A17) yields

$$l_2 = \frac{u_e' f_e'' - u_e'' f_e'}{u_e' v_e'' - u_e'' v_e'} = \frac{2\cosh^2 q + 1}{p \sinh q} - \frac{3\cosh q}{p^2}.$$

(A18)

$$l_1 = \frac{f_e v_e' - f_e' v_e}{u_e v_e' - u_e' v_e} = -\frac{\cosh^2 q + 5}{2p \tanh q} + \frac{6\cosh^2 q + 3}{2p^2}.$$

(A19)

$$l_0 = f_e - u_e l_1 - v_e l_2 = 1 - \frac{3\coth q}{2p} + \frac{3}{2p^2}.$$

(A20)

To determine the general expressions for the coefficients κ_k (k = 0, 1, 2), expansions (A8)-(A10) are substituted into (A2), and coefficients of $(r_e - r_0)^0$, $(r_e - r_0)^1$, and $(r_e - r_0)^2$ are matched on both sides, giving

$$k_0 + u_e k_1 + v_e k_2 = g_e.$$

(A21)

$$u_e' k_1 + v_e' k_2 = g_e'.$$

(A22)

$$u_e'' k_1 + v_e'' k_2 = g_e''.$$

(A23)

Solving (A21) -(A23) gives the expansion coefficients

$$k_2 = \frac{u_e g_e' - u_e' g_e}{u_e v_e' - u_e' v_e} = k_a (3\coth q \cosh q - \sinh q) + k_b \cosh q.$$

(A24)

$$k_1 = \frac{g_e v_e' - g_e' v_e}{u_e v_e' - u_e' v_e} = -k_a \left(3\coth q \cosh^2 q - \frac{5}{4}\sinh 2q\right) + \frac{1}{2} k_b (\cosh^2 q + 1),$$

(A25)

$$k_0 = \tanh\left(\tfrac{1}{2} p\right) - \frac{3}{2} k_a \coth q - k_b \left(2\coth^2 q - \frac{1}{2}\right),$$

(A26)

where

$$k_a = \frac{1}{2}\operatorname{sech}^2\left(\tfrac{1}{2} p\right) - \frac{\tanh\left(\tfrac{1}{2} p\right)}{p},$$

(A27)

$$k_b = -\frac{1}{2}\operatorname{sech}^2\left(\tfrac{1}{2}p\right)\tanh\left(\tfrac{1}{2}p\right) - \frac{\operatorname{sech}^2\left(\tfrac{1}{2}p\right)}{p} + \frac{2\tanh\left(\tfrac{1}{2}p\right)}{p^2}.$$

(A28)

Appendix B

This appendix provides the detailed derivation of the potential parameters α, q, U_0, U_1, and U_2. For convenience, the EPT potential defined in equation (2) is rewritten in the more tractable form

$$U(r)=U_0+\frac{1}{y^2}U_1-\frac{x}{y^2}U_2,$$

(B1)

where the auxiliary functions are

$$x=\cosh a(r-r_0),$$

(B2)

$$y=\sinh a(r-r_0).$$

(B3)

Equations (B1) -(B3) are connected through the identity $x^2-y^2=1$, which is used repeatedly in subsequent simplifications. To enforce the boundary condition (29a), note that in the limit $\rho\to\infty$, both $x\to\infty$ and $y\to\infty$. Consequently, $1/y^2\to 0$, $x/y^2\to 0$, and applying these limits to (B1) gives

$$\lim_{r\to\infty}U(r)=U_0.$$

(B4)

At the equilibrium point $\rho=\rho_e$, substituting (B2) and (B3) into (B1) yields

$$U(r_e)=U_0+\frac{1}{y_e^2}U_1-\frac{x_e}{y_e^2}U_2,$$

(B5)

where

$$x_e=\cosh a(r_e-r_0),$$

(B6)

$$y_e=\sinh a(r_e-r_0).$$

(B7)

Inserting (B4) and (B5) into condition (29a) leads to

$$-U_1 + x_e U_2 = y_e^2 D_e.$$

(B8)

To satisfy the derivative-based conditions (29b) -(29d), direct differentiation of (2) with respect to ρ is algebraically unwieldy. A more manageable approach is to work from the total differential of U(ρ)

$$\frac{dU}{dr} = \frac{\partial U}{\partial x}\frac{dx}{dr} + \frac{\partial U}{\partial y}\frac{dy}{dr}.$$

(B9)

Differentiating (B2) and (B3) gives

$$\frac{dx}{dr} = a \sinh a(r - r_0) \equiv a y.$$

(B10)

$$\frac{dy}{dr} = a \cosh a(r - r_0) \equiv a x.$$

(B11)

Substituting (B10) and (B11) into (B9) yields the differential operator used to generate successive derivatives of the potential

$$\frac{d}{dr} = a\left(y\frac{\partial}{\partial x} + x\frac{\partial}{\partial y}\right).$$

(B12)

Applying this operator to (B1) produces the first derivative

$$U'(r) = \frac{d}{dr}U \equiv a\left(-\frac{2x}{y^3}U_1 + \frac{2x^2 - y^2}{y^3}U_2\right).$$

(B13)

To simplify further differentiation, the identity $y^2 = x^2 - 1$ is applied to (B13) so that the numerator depends only on x, and the denominator only on y, giving

$$U'(r) = a\left(-\frac{2x}{y^3}U_1 + \frac{x^2+1}{y^3}U_2\right).$$

(B14)

Evaluating at $\rho = \rho_e$ (where $x = x_e$, $y = y_e$), and applying condition (29b), results in

$$-2x_e U_1 + \left(2x_e^2 - y_e^2\right) U_2 = 0.$$

(B15)

Solving the linear system formed by (B8) and (B15) yields

$$U_1 = \left(x_e^2 + 1\right) D_e.$$

(B16)

$$U_2 = 2x_e D_e.$$

(B17)

Next, applying operator (B12) to (B14) gives the second derivative

$$U''(r) = a^2 \left(\frac{4x^2 + 2}{y^4} U_1 - \frac{x^3 + 5x}{y^4} U_2 \right).$$

(B18)

At equilibrium $\rho = \rho_e$, using (B16), (B17), (B18) with condition (29c) produces

$$U''(r_e) = 2a^2 D_e.$$

(B19)

$$a = \pi c w_e \sqrt{\frac{2m}{D_e}}.$$

(B20)

Proceeding similarly, the third derivative at equilibrium is obtained as

$$U'''(r_e) = -6a^3 D_e \frac{x_e}{y_e} = -6a^3 D_e \coth a\left(r_e - r_0\right).$$

(B21)

Combining (B19), (B21), and condition (29d), and solving gives

$$r_0 = r_e - \frac{1}{a} \ln \sqrt{\left| \frac{1 + \frac{a_e w_e}{6B_e^2} + a r_e}{1 + \frac{a_e w_e}{6B_e^2} - a r_e} \right|},$$

(B22)

where $|x|$ denotes the absolute value of x.

The Varshni conditions determine expressions for U_1, U_2, α, and ρ_0, but do not yield a direct formula for U_0. To obtain U_0, the constraint $U(\rho_e) = 0$ is imposed

on the potential, giving $U_0 = D_e$. This choice shifts the potential minimum to zero without altering the physical observables of the system [48]. The motivation for this constraint is: (a) It standardizes the reference energy for comparison with other diatomic oscillator models. (b) It preserves all thermodynamic and spectroscopic properties of the modeled system. This convention ensures that the equilibrium minimum of the EPT oscillator is fixed at zero potential while maintaining consistency with established results in the literature.

References

[1] Sema, C. N., Garcia, N. A. & Camperos, J. A. G. Applications of thermodynamics to study the physical phenomena of heat conduction. *J. Phys. Conf. Ser.* 2073, 012010. https://doi.org/10.1088/1742-6596/2073/1/012010 (2024).

[2] Haddad, W. M. Condensed matter physics, hybrid energy and entropy principles, and the hybrid first and second laws of thermodynamics. *Commun. Nonlinear Sci. Numer. Simul.* 83, 105096. https://doi.org/10.1016/j.cnsns.2019.105096 (2020).

[3] Wang, J. F., Zhang, H., Liang, L. X., Peng, X. L., Wang, C. W., Deng, P., Ding, Q. C. & Jia, C. S. A novel formulation representation regarding the equilibrium constant subject to reactions between N_2 and O_2. *Comput. Theor. Chem.* 1239, 114758. https://doi.org/10.1016/j.comptc.2024.114758 (2024).

[4] Ebeler, M., Pilgram, F., Wellhoefer, T., Frankenfeld, K. & Franzreb, M. First comprehensive view on a magnetic separation-based protein purification process: from process development to cleaning validation of a GMP-ready magnetic separator. *Eng. Life Sci.* 19, 591. https://doi.org/10.1002/elsc.201800183 (2019).

[5] Liao, Z., Han, L., Li, Q., Li, L., Liu, Y., Song, Y., Tan, W. & Song, E. Gradient magnetic separation and fluorescent imaging-based heterogeneous circulating tumor cell subpopulations assay with biomimetic multifunctional nanoprobes. *Adv. Funct. Mater.* 31, 2009937. https://doi.org/10.1002/adfm.202009937 (2021).

[6] Pringle, J. K., Giubertoni, M., Cassidy, N. J., Wisniewski, K. D., Hansen, J. D., Linford, N. T. & Daniels, R. M. The use of magnetic susceptibility as a forensic search tool. *Forensic Sci. Int.* 246, 31. https://doi.org/10.1016/j.forsciint.2014.10.046 (2016).

[7] Ayoubi, S., Adman, V. & Yousefifard, M. Use of magnetic susceptibility to assess metals concentration in soils developed on a range of parent materials. *Ecotoxicol. Environ. Saf.* 168, 138. https://doi.org/10.1016/j.ecoenv.2018.10.024 (2019).

[8] Khordad, R. Stark shift in a Frost-Musulin quantum dot: analytical solution. *Phys. B* 690, 416297. https://doi.org/10.1016/j.physb.2024.416297 (2024).

[9] Onate, C. A., Okon, I. B., Omugbe, E., Eyube, E. S., Al-Asbahi, B. A., Kumar, Y. A., Emeje, K. O., Aghemenloh, E., Obasuyi, A. R., Obaje, V. O. & Etchie, T. O. Theoretical prediction of molar entropy of modified shifted Morse potential for gaseous molecules. *Chem. Phys.* 582, 112294. https://doi.org/10.1016/j.chemphys.2024.112294 (2024).

[10] Douici, M., Boukabcha, H. & Rermous, R. Study of energy spectra and thermodynamic properties of the relativistic Dirac equation using the Feynman path integral method. *Phys. Scr.* 98, 075405. https://doi.org/10.1088/1402-4896/acdc60 (2023).

[11] Valencia-Ortega, G. & Arias-Hernandez, L. A. Thermodynamic properties of diatomic molecule systems under SO(2,1)-anharmonic Eckart potential. *Int. J. Quantum Chem.* 118, e25589. https://doi.org/10.1002/qua.25589 (2018).

[12] Sharipov, A. S., Loukhovitski, B. I. & Starik, A. M. Influence of vibrations and rotations of diatomic molecules on their physical properties. *J. Phys. B: At. Mol. Opt. Phys.* 49, 125103. https://doi.org/10.1088/0953-4075/49/12/125103 (2016).

[13] Omugbe, E., Osafile, O. E., Okon, I. B., Okorie, U. S., Suleman, K. O., Njoku, I. J., Jahanshir, A. & Onate, C. A. Influence of external magnetic and Aharonov-Bohm flux fields on bound states of the Klein-Gordon and Schroedinger equations via the SWKB approach. *Eur. Phys. J. D* 76, 177. https://doi.org/10.1140/epjd/s10053-022-00507-2 (2022).

[14] Eyube, E. S., Nyam, G. G., Notani, P. P., Izam, M. M. & Jabil, Y. Y. Energy spectrum and magnetic properties of the Tietz oscillator in external magnetic and Aharonov-Bohm flux fields. *Indian J. Phys.* 98, 55. https://doi.org/10.1007/s12648-023-02811-y (2024).

[15] Ikot, A. N., Edet, C. O., Amadi, P. O., Okorie, U. S., Rampho, G. J. & Abdullah, H. Y. Thermodynamic properties of Aharonov-Bohm and magnetic fields with the screened Kratzer potential. *Eur. Phys. J. D* 74, 159. https://doi.org/10.1140/epjd/e2020-10084-9 (2020).

[16] Eyube, E. S., Yusuf, I., Omugbe, E., Makasson, C. R., Onate, C. A., Mohammed, B. D., Balami, B. Y. & Tahir, A. M. Energy spectrum and magnetic susceptibility of the improved Poschl-Teller potential. *Phys. B* 694, 416483. https://doi.org/10.1016/j.physb.2024.416483 (2024).

[17] Horchani, R., Al-Aamri, H., Al-Kindi, S., Ikot, A. N., Okorie, U. S., Rampho, G. J. & Jelassi, H. Energy spectra and magnetic properties of diatomic molecules in magnetic and Aharonov-Bohm fields with the inversely quadratic Yukawa potential. *Eur. Phys. J. D* 75, 36. https://doi.org/10.1140/epjd/s10053-021-00038-2 (2021).

[18] Eyube, E. S., Notani, P. P., Onate, C. A., Wadata, U., Bitrus, B. M. & Najoji, S. D. Energy eigenvalues and finite temperature magnetization for the improved Scarf II potential in external magnetic and Aharonov-Bohm flux fields. *Heliyon* 9, e20848. https://doi.org/10.1016/j.heliyon.2023.e20848 (2023).

[19] Ma, Z. Q. & Xu, B. W. Quantum correction in exact quantization rules. *EPL* 69, 685. https://doi.org/10.1209/epl/i2004-10418-8 (2005).

[20] Serrano, F. A., Gu, X. Y. & Dong, S. H. Proper quantization rule and applications to exactly solvable quantum systems. *J. Math. Phys.* 51, 082103. https://doi.org/10.1063/1.3466802 (2010).

[21] Ahmadov, A. I., Demirci, M. & Aslanova, S. M. Bound state solutions of the Klein-Gordon equation with the sum of Manning-Rosen and Yukawa potentials within SUSYQM. *J. Phys. Conf. Ser.* 1416, 012001. https://doi.org/10.1088/1742-6596/1416/1/012001 (2019).

[22] Tsaur, G. Y. & Wang, J. Integration of the Schrödinger equation by canonical transformations. *Phys. Rev. A* 65, 012104. https://doi.org/10.1103/PhysRevA.65.012104 (2001).

[23] Ikot, A. N., Amadi, P. O., Okorie, U. S., Horchani, R., Okpara, N. & Obagboye, L. Energy levels for the improved generalized Pöschl-Teller oscillator. *EPL* 142, 50003. https://doi.org/10.1209/0295-5075/acd57d (2023).

[24] Ghobrini, A., Boukabcha, H. & Ami I. Energy spectra with the Dirac equation of the q-deformed generalized Pöschl-Teller potential via the Feynman approach for $^{39}K_2$ (a $^3\Sigma_u^+$). *J. Mol. Model.* 30, 340. https://doi.org/10.1007/s00894-024-06139-0 (2024)

[25] Ghobrini, A., Boukabcha, H., Ami, I. & Hajigeorgiou, P. G. Path integral solutions of the Dirac equation for the generalized Pöschl-Teller model: application to the CO molecule. *Eur. Phys. J. D* 79, 64. https://doi.org/10.1140/epjd/s10053-025-01013-4 (2025).

[26] Atman, K.G., & Hüseyin Şirin, H. Nonlocal phenomena in quantum mechanics with fractional calculus. *Rep. Math. Phys*. 86, 263 (2020). https://doi.org/10.1016/S0034-4877(20)30075-6

[27] Suparmi, A., Permatahati, L.K., Marzuki, A. & Cari C. Study of the fractional Schrödinger equation with Morse potential and the optical properties of quantum dots under the magnetic field *Eur. Phys. J. Plus* 139, 529. https://doi.org/10.1140/epjp/s13360-024-05323-8 (2024).

[28] Partohaghighi, M., Mirtalebi, Z., Akgül, A. & Riaz, M.B. Fractal-fractional Klein-Gordon equation: A numerical study *Result Phys* 42, 105970 https://doi.org/10.1016/j.rinp.2022.105970 (2022).

[29] Boulaaras, S., Jan, R. & Pham, V.T. Recent advancement of fractional calculus and its applications in physical systems. *Eur. Phys. J. Spec. Top*. 232, 2347 https://doi.org/10.1140/epjs/s11734-023-01002-4 (2023).

[30] Godinho, C. F. d. L., & Vancea, I. V. V. Fractional Calculus in Physics: A Brief Review of Fundamental Formalisms. *Mathematics*, 13, 3643 (2025). https://doi.org/10.3390/math13223643

[31] Laskin, N. (2018). Nonlocal Quantum Mechanics: Fractional Calculus Approach. De Gruyter Brill. https://www.degruyter.com/document/doi/10.1515/9783110571721-009/html

[32] L. Y. Medina, J. D. Correa, M. E. Mora-Ramos, and J. F. Pérez-Torres, “Application of Laskin Fractional Quantum mechanics with a changed fractional differential operator to one-dimensional potentials,” Revista Mexicana de Física, vol. 71, no. 2 (Mar-Apr 2025), article 020703, https://doi.org/10.31349/RevMexFis.71.020703

[33] Abu-Shady, M., Khokha, E.M. & Abdel-Karim, T.A. The generalized fractional NU method for the diatomic molecules in the Deng-Fan model *Eur. Phys. J. D*. 76, 159 https://doi.org/10.1140/epjd/s10053-022-00480-w (2022)

[34] Abu-Shady, M. & Khokha, E.M. On prediction of the fractional vibrational energies for diatomic molecules with the improved Tietz potential *Mol. Phys.* 120, e2140720 https://doi.org/10.1080/00268976.2022.2140720 (2022).

[35] Abu-Shady, M. & Khokha, E.M. A precise estimation for vibrational energies of diatomic molecules using the improved Rosen-Morse potential *Sci. Rep*. 13, 11578 https://doi.org/10.1038/s41598-023-37888-2 (2023).

[36] Abu-Shady, M. & Fath-Allah, H.M. The parametric generalized fractional Nikiforov-Uvarov method and its applications *East Eur. J. Phys*. 3, 248 https://doi.org/10.26565/2312-4334-2023-3-22 (2023).

[37] Pöschl, G. & Teller, E. Bemerkungen zur Quantenmechanik des anharmonischen Oszillators. *Z. Physik* 83:143. https://doi.org/10.1007/BF01331132 (1933).

[38] Eyube, E.S., Notani, P.P. & Dikko, A.B. Modeling of diatomic molecules with modified hyperbolical-type potential *Eur. Phys. J. Plus* 137, 329 https://doi.org/10.1140/epjp/s13360-022-02526-9 (2022).

[39] Hachama, M. & Diaf, A. Ro-vibrational relativistic states for the q-deformed hyperbolic barrier potential *Eur. Phys. J. Plus* 139:501 https://doi.org/10.1140/epjp/s13360-024-05284-y (2024).

[40] Eyube, E.S. Prediction of thermal properties of phosphorus dimer-The analytical approach *Chem. Phys. Lett*. 801, 139702 https://doi.org/10.1016/j.cplett.2022.139702 (2022).

[41] Eyube, E.S., Bitrus, B.M. & Jabil, Y.Y. Thermodynamic relations and ro-vibrational energy levels of the improved Pöschl-Teller oscillator for diatomic molecules *J. Phys. B: At. Mol. Opt. Phys*. 54:155102 https://doi.org/10.1088/1361-6455/ac00c5 (2021)

[42] Yanar, H. Comments on thermodynamic relations and ro-vibrational energy levels of the improved Pöschl-Teller oscillator for diatomic molecules *J. Phys. B: At. Mol. Opt. Phys*. 55, 178001 https://doi.org/10.1088/1361-6455/ac8212 (2021).

[43] Pingak, R.K., Johannes, A.Z., Ngara, Z.S., Bukit, M., Nitti, F., Tambaru, D., & Ndii, M.Z. Accuracy of Morse and Morse-like oscillators for diatomic molecular interaction: A comparative study. *Results Chem*. 3, 100204 (2021). https://doi.org/10.1016/j.rechem.2021.100204

[44] Lotliker, S.U., Samant, R., Mesquita, N., Liu, D. & Desai, A.M. Accuracy of the new modified Morse potential energy function for ground and excited states of diatomic molecules, *Open Phys*. 16, 100159. https://doi.org/10.1016/j.physo.2023.100159 (2023).

[45] Ahmed, A.D., Eyube, E.S., Onate, C.A., Amasuwa, S., Omugbe, E. & Balami, B.Y. Nonrelativistic bound-state energy spectrum and persistent current in the modified Rosen-Morse oscillator confined to a 2D electromagnetic potential field *Eur. Phys. J. D* 78, 6 https://doi.org/10.1140/epjd/s10053-024-00802-0 (2024).

[46] Eyube, E.S., Tanko, P.U., Notani, P.P., Yabwa, D., Bitrus, B.M., Wadata, U. & Samaila, H. Analytical energy levels of the Schrödinger equation for the improved generalized Pöschl-Teller oscillator with magnetic vector potential coupling *Eur. Phys. J. D* 77, 88 https://doi.org/10.1140/epjd/s10053-023-00666-w (2023).

[47] Pekeris, C.L. The rotation-vibration coupling in diatomic molecules. *Phys. Rev*. 45:98. https://doi.org/10.1103/PhysRev.45.98 (1934).

[48] Yanar, H., Taş, A., Salti, M. & Aydoğdu, O. Ro-vibrational energies of CO molecule via improved generalized Pöschl-Teller potential and Pekeris-type approximation *Eur. Phys. J. Plus* 135, 292 https://doi.org/10.1140/epjp/s13360-020-00297-9 (2020).

[49] Ahmed, A.D., Eyube, E.S., Omaghali, N.E.J., Inuwa, A. & Makama, M.K. Energy levels and thermodynamic models of the general molecular oscillator under a 2D electromagnetic potential field *Phys. Scr*. 99, 115013 https://doi.org/10.1088/1402-4896/ad827c (2024).

[50] Schwabl, F. Statistical Mechanics, 2nd ed. (Springer, Berlin, 2006)

[51] Boyacioglu, B. & Chatterjee, A. Dia- and paramagnetism and total susceptibility of GaAs quantum dots with Gaussian confinement *Phys. E* 44, 1826 https://doi.org/10.1016/j.physe.2012.05.001 (2012).

[52] Molpeceres, G., Furuya, K. & Aikawa, Y. Enhanced formation of interstellar complex organic molecules on carbon monoxide ice. *Astron. Astrophys.* 688, A150. https://doi.org/10.1051/0004-6361/202449604 (2024).

[53] Langen, T., Valtolina, G., Wang, D. & Ye, J. Quantum state manipulation and cooling of ultracold molecules. *Nat. Phys*. 20, 702. https://doi.org/10.1038/s41567-024-02423-1 (2024).

[54] Singh, J., Tennyson, J., Longiany, G. & Korpal, S. R-matrix calculation of electron collisions with the ICl molecule. *Chem. Phys*. 580, 112208. https://doi.org/10.1016/j.chemphys.2024.112208 (2024).

[55] Chen, X.Y., Biswas, S., Eppelt, S., Schindewolf, A., Deng, F., Shi, T., Yi, S., Hilker, T.A., Bloch, I. & Luo, X.Y. Ultracold field-linked tetratomic molecules. *Nature* 626, 283 https://doi.org/10.1038/s41586-023-06986-6 (2024).

[56] Hajigeorgiou, P.G. An extended Lennard-Jones potential energy function for diatomic molecules: Application to ground electronic states *J. Mol. Spectrosc*. 263, 101 https://doi.org/10.1016/j.jms.2010.07.003 (2010).

[57] Li, D., Xie, F. & Li, L. Observation of the Cs_2 $3^3\Sigma_g^+$ state by infrared-infrared double resonance *Chem. Phys. Lett*. 458, 267 https://doi.org/10.1016/j.cplett.2008.04.115 (2008).

[58] Coxon, J.A. & Wicramaaratchi, M.A. The $A^3\Pi(1) \rightarrow X^1\Sigma^+$ emission spectrum of ICl in the near infrared *J. Mol. Spectrosc*. 79, 380 https://doi.org/10.1016/0022-2852(80)90220-9 (1980).

[59] Li, D., Xie, F., Li, L., Lazoudis, A. & Lyyra, A.M. New observation of the $^6Li^7Li$, $3^3\Sigma_g^+$, $1^3\Delta_g$, and 2 $^3\Pi_g$ states and molecular constants with all $^6Li_2$, $^7Li_2$, and $^6Li^7Li$ data *Mol. Spectrosc*. 246, 180 https://doi.org/10.1016/j.jms.2007.09.008 (2007).

[60] Jastrzebski, W., Kowalczyk, P., Camacho, J.J., Pardo, A. & Poyato, J.M.L. The C(2) $^1\Pi_u$ state of Na_2 molecule studied by polarization labelling spectroscopy method *Spectrochim. Acta –A: Mol. Biomol. Spectrosc*. 57, 1829 https://doi.org/10.1016/S1386-1425(01)00405-X (2001).

[61] Feber, R., Pazyuk, E.A., Stolyarov, A.V., Zaitsevskii, A., Kowalczyk, P., Chen, H., Wang, H. & Stwalley, W.C. The c $^3\Sigma^+$, b $^3\Pi$, and a $^3\Sigma^+$ states of NaK revisited *J. Chem. Phys*. 112, 5740 https://doi.org/10.1063/1.481149 (2000).

[62] Varshni, Y.P. *Rev. Mod. Phys*. 29: 664 https://doi.org/10.1103/RevModPhys.29.664 (1957).

[63] Kirschner, S.M. & Watson, J.K.G. Second-order semiclassical calculations for diatomic molecules *J. Mol. Spectrosc*. 51, 321 https://doi.org/10.1016/0022-2852(74)90060-5G (1974).

[64] Onate, C.A., Okon, I.B., Eyube, E.S., Bankole, D.T., Omugne, E., Olayinka, A.S., Onyeaju, M.C., Ebomwonyi, O. & Odeyemi, O.E. Analytical study of gallium halides for Pöschl-Teller potential model *Chem. Phys. Impact*. 5, 100123 https://doi.org/10.1016/j.chphi.2022.100123 (2022).

[65] Mustafa, O. On the ro-vibrational energies for the lithium dimer; maximum-possible rotational levels *J. Phys. B. At. Mol. Opt. Phys*. 48, 065101 https://doi.org/10.1088/0953-4075/48/6/065101 (2015).

[66] Liu, J.Y., Hu, X.T. & Jia, C.S. Molecular energies of the improved Rosen-Morse potential energy model *Can. J. Chem*. 92, 40 https://doi.org/10.1139/cjc-2013-0396 (2014).

[67] Eyube, E.S., Timtere, P. & Yerima, J.B. Potential parameters, ro-vibrational energy spectra, and expectation values of the improved deformed exponential-type potential *Can. J. Phys*. 100, 351 https://doi.org/10.1139/cjp-2020-0513 (2022).

[68] Eyube, E.S., Notani, P.P. & Izam, M.M. Potential parameters and eigen spectra of improved Scarf II potential energy function for diatomic molecules *Mol. Phys*. 120, e1979265 https://doi.org/10.1080/00268976.2021.1979265 (2022).

[69] Eyube, E.S., Samaila, H., Okon, I.B., Tanko, P.U., Onate, C.A., Yabwa, D., Notani, P.P. & Omugbe, E. Energy levels of the improved Tietz oscillator in external magnetic and Aharonov-Bohm flux fields: the Pekeris approximation recipe *Eur. Phys. J. Plus* 138, 251 https://doi.org/10.1140/epjp/s13360-023-03830-8 (2023).

[70] Hu, X.T., Liu, J.Y. & Jia, C.S. The 3 $^{3}\Sigma_{g}^{+}$ state of Cs_2 molecule *Comp. Theor. Chem*. 1019, 137 https://doi.org/10.1016/j.comptc.2013.06.020 (2013).

[71] Eyube, E.S., Nyam, G.G. & Notani, P.P. Improved q-deformed Scarf II oscillator *Phys. Scr*. 96, 125017 https://doi.org/10.1088/1402-4896/ac2eff (2021).

[72] Eyube, E.S. Reparameterised Pöschl-Teller oscillator and analytical molar entropy equation for diatomic molecules *Mol. Phys*. 120, e2037774 https://doi.org/10.1080/00268976.2022.2037774 (2022).

List of Tables

Table 1: Input data for the diatomic molecules investigated in this study

Diatomic molecule	**Molecular state**	**Molecular constant [[56], [57], [58], [59], [60], [61]]**				**Potential constant**	
		D_e (cm^{-1})	ω_e (cm^{-1})	$\alpha_e/10^{-4}$ (cm^{-1})	ρ_e (Å)	ρ_0 (Å)	α ($Å^{-1}$)
CO	X $^1\Sigma^+$	90670	2169.8129	175.0406	1.12832320	0.2744	2.2978
Cs_2	3 $^3\Sigma_g^+$	2722.28	28.8918	0.28103	5.3474208	2.3942	0.5497
ICl	X $^1\Sigma_g^+$	17557.6	384.27	5.32	2.32091	1.6435	1.8591
$^7Li_2$	1 $^3\Delta_g$	9709.511	279.8128	52.844	3.0167036	-0.0736	0.6477
Na_2	C(2) $^1\Pi_u$	5573	116.310	8.7745	3.5503	-0.3117	0.6433
NaK	c $^3\Sigma^+$	2508.0	73.4	5.91425	4.3075	1.2537	0.6787

Table 2: Vibrational state energies of molecules: Calculations with and without fractional parameters compared to RKR data

CO ($X\ ^1\Sigma^+$)						**Cs_2 ($3\ ^3\Sigma_g^+$)**					
n **[63]**	Energy (cm^{-1}), a = 0.6102, C = 0.5040			PAD (%)		n [57]	Energy (cm^{-1}), a = 0.6101, C = 0.5025			PAD (%)	
	Eq. (18)	Eq. (19)	RKR [63]	Eq. (18)	Eq. (19)		Eq. (18)	Eq. (19)	RKR [57]	Eq. (18)	Eq. (19)
0	1080.8915	1081.4457	1081.7791	0.0820	0.0308	0	14.4446	14.4277	14.4248	0.1376	0.0204
1	3223.6581	3225.2967	3225.0522	0.0432	0.0076	1	43.2166	43.1662	43.1680	0.1125	0.0041
2	5340.4885	5343.1849	5341.8437	0.0254	0.0251	2	71.8348	71.7514	71.7657	0.0963	0.0200
3	7431.3826	7435.1103	7432.2200	0.0113	0.0389	3	100.2994	100.1832	100.2211	0.0781	0.0378
4	9496.3407	9501.0730	9496.2494	0.0010	0.0508	4	128.6103	128.4617	128.5375	0.0566	0.0589
5	11535.3625	11541.0729	11534.0013	0.0118	0.0613	5	156.7675	156.5870	156.7182	0.0315	0.0837
...	...	...	...	...	...	6	184.7711	184.5589	184.7663	0.0026	0.1123
32	56785.0736	56807.1451	56909.6553	0.2189	0.1801	7	212.6210	212.3774	212.6851	0.0301	0.1447
33	58097.8823	58120.1876	58240.4388	0.2448	0.2065	8	240.3172	240.0427	240.4778	0.0668	0.1809
34	59384.7547	59407.2673	59550.0742	0.2776	0.2398	9	267.8597	267.5547	268.1477	0.1074	0.2212
35	60645.6910	60668.3842	60835.5899	0.3122	0.2748	10	295.2486	294.9133	295.6980	0.1520	0.2654
36	61880.6910	61903.5384	62097.0060	0.3484	0.3116	11	322.4838	322.1186	323.1320	0.2006	0.3136
37	63089.7549	63112.7298	63334.3337	0.3662	0.3499	12	349.5653	349.1706	350.4529	0.2533	0.3659
MPAD (%)				0.0905	0.0990	MPAD (%)				0.1020	0.1407

Table 3: Vibrational state energies of molecules: Calculations with and without fractional parameters compared to RKR data

ICl (X $^1\Sigma_g^+$)						**$^7Li_2$ (1 $^3\Delta_g$)**					
n **[58]**	Energy (cm^{-1}), a = 0.6200, C = 0.5007			PAD (%)		n [59]	Energy (cm^{-1}), a = 0.6300, C = 0.5010			PAD (%)	
	Eq. (18)	Eq. (19)	RKR [63]	Eq. (18)	Eq. (19)		Eq. (18)	Eq. (19)	RKR [57]	Eq. (18)	Eq. (19)
0	194.04	191.78	191.76	1.1874	0.0107	0	142.0238	139.3090	139.5361	1.7829	0.1627
1	578.50	571.84	573.03	0.9550	0.2071	1	423.0935	415.0909	416.0048	1.7040	0.2197
2	958.66	947.70	951.28	0.7762	0.3762	2	699.9727	686.8408	689.1511	1.5703	0.3352
3	1334.52	1319.35	1326.50	0.6047	0.5387	3	972.6616	954.5589	958.9954	1.4251	0.4626
4	1706.07	1686.80	1698.66	0.4364	0.6981	4	1241.1601	1218.2450	1225.5553	1.2733	0.5965
5	2073.32	2050.04	2067.75	0.2695	0.8563	5	1505.4683	1477.8993	1488.8460	1.1165	0.7352
6	2436.27	2409.08	2433.74	0.1038	1.0132	...	...	...	...	...	...
7	2794.91	2763.91	2796.61	0.0609	1.1692	20	4967.2466	4888.8879	5048.2931	1.6054	3.1576
8	3149.24	3114.54	3156.35	0.2252	1.3246	21	5164.5089	5084.0321	5259.2289	1.8010	3.3312
9	3499.27	3460.96	3512.93	0.3887	1.4793	22	5357.5808	5275.1444	5466.7580	1.9971	3.5051
10	3845.00	3803.18	3866.34	0.5519	1.6336	23	5546.4624	5462.2248	5670.8492	2.1934	3.6789
11	4186.43	4141.19	4216.55	0.7144	1.7872	24	5731.1535	5645.2733	5871.4685	2.3898	3.8524
12	4523.54	4475.00	4563.55	0.8766	1.9404	25	5911.6544	5824.2900	6068.5795	2.5859	4.0255
MPAD (%)				0.5501	1.0027	MPAD (%)				1.1756	1.9504

Table 4: Vibrational state energies of molecules: Calculations with and without fractional parameters compared to RKR Data

Na_2 ($C(^2)\ ^1\Pi_u$)						**NaK ($c\ ^3\Sigma^+$)**					
n **[60]**	Energy (cm^{-1}) $a = 0.6040$, $C = 0.5001$			PAD (%)		*n* [61]	Energy (cm^{-1}) $a = 0.6200$, $C = 0.5000$			PAD (%)	
	Eq. (18)	Eq. (19)	RKR [63]	Eq. (18)	Eq. (19)		Eq. (18)	Eq. (19)	RKR [57]	Eq. (18)	Eq. (19)
0	57.901	57.979	58.005	0.1801	0.0456	0	37.02	36.56	36.59	1.1686	0.0852
1	172.844	173.075	173.023	0.1037	0.0301	1	110.24	108.88	109.02	1.1164	0.1240
2	286.576	286.958	286.764	0.0655	0.0676	2	182.36	180.14	180.49	1.0335	0.1958
3	399.099	399.627	399.242	0.0359	0.0964	3	253.37	250.31	250.98	0.9533	0.2652
4	510.410	511.082	510.472	0.0121	0.1195	4	323.29	319.42	320.49	0.8732	0.3344
5	620.512	621.324	620.468	0.0070	0.1379	5	392.10	387.45	389.02	0.7926	0.4041
6	729.403	730.352	729.244	0.0217	0.1519	…	…	…	…	…	…
7	837.083	838.166	836.815	0.0320	0.1614	31	1794.77	1779.22	1804.95	0.5641	1.4256
8	943.553	944.766	943.196	0.0378	0.1665	32	1833.85	1818.25	1844.60	0.5827	1.4286
9	1048.813	1050.153	1048.401	0.0393	0.1671	33	1871.83	1856.20	1883.09	0.5978	1.4278
10	1152.862	1154.326	1152.445	0.0362	0.1632	34	1908.71	1893.09	1920.44	0.6106	1.4244
11	1255.700	1257.286	1255.343	0.0285	0.1548	35	1944.49	1928.89	1956.61	0.6193	1.4166
12	1357.329	1359.031	1357.106	0.0164	0.1419	36	1979.17	1963.63	1991.62	0.6251	1.4056
MPAD (%)				0.0474	0.1234	MPAD (%)				0.4840	0.9811

Table 5: Comparative analysis of MPAD (%) data for diatomic molecules

Energy model	**Diatomic molecules**					
	CO ($X\ ^1\Sigma^+$)	Cs_2 ($3\ ^3\Sigma_g^+$)	ICl ($X\ ^1\Sigma_g^+$)	$^7Li_2$ ($1\ ^3\Delta_g$)	Na_2 ($C(2)\ ^1\Pi_u$)	NaK ($c\ ^3\Sigma^+$)
EPT	0.0905	0.1020	0.5501	1.1756	0.0474	0.4840
[a]MHT	0.1002 [38]	...	...	...	...	...
[b]IGPT	0.0990 [48]	...	...	...	...	...
[c]MOR	0.0989 [48]	0.1407 [66]	1.0163 [67]	...	...	0.9796 [67]
[d]IS	0.0991 [68]	...	...	...	0.1240 [68]	0.9799 [68]
[e]IT	0.3985 [69]	0.0412 [34] 0.0414 [70]	0.5945 [67]	1.6826 [49]	...	0.6653 [67]
[f]IRM	...	0.0414 [66]	...	1.1520 [49]	...	...
[g]IMR				3.9066 [49]		
[h]DS	...	...	1.0292 [71]	...	...	...
[i]SPT	...	...	...	...	0.1257 [72]	...
[j]DPT	...	...	...	...	0.1250 [72]	...

a: Energy model for the hyperbolic-type (MHT) oscillator

b: Energy model for the Improved generalized Pöschl-Teller (IGPT) oscillator

c: Energy model for the Morse (MOR) oscillator

d: Energy model for the Improved Scarf (IS) oscillator

e: Energy model for the Improved Tietz (IT) oscillator

f: Energy model for the Improved Rosen-Morse (IRM) oscillator

g: Energy model for the Improved Manning-Rosen (IMR) oscillator

h: Energy model for the deformed Scarf (DS) oscillator

i: Energy model for the specialized Pöschl-Teller (SPT) oscillator

j: Energy model for the deformed Pöschl-Teller (DPT) oscillator

List of Figures

Figure 1: Comparison of the Pekeris-type approximation (f_{appr}) with the exact function (f) for the CO ($X\ ^1\Sigma^+$) molecule. The plot illustrates the fit of the approximation to the exact function

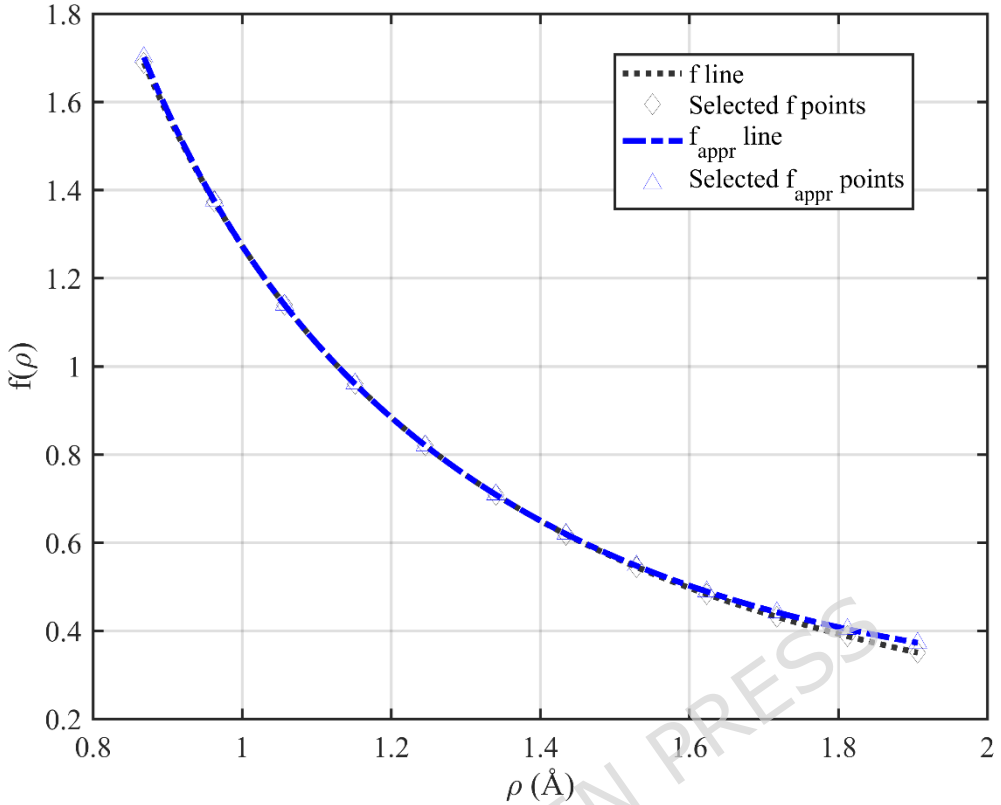

Figure 2: Comparison of the Pekeris-type approximation (f_{appr}) with the exact function (f) for the Cs_2 ($3\ ^3\Sigma_g^+$) molecule. The plot illustrates the fit of the approximation to the exact function

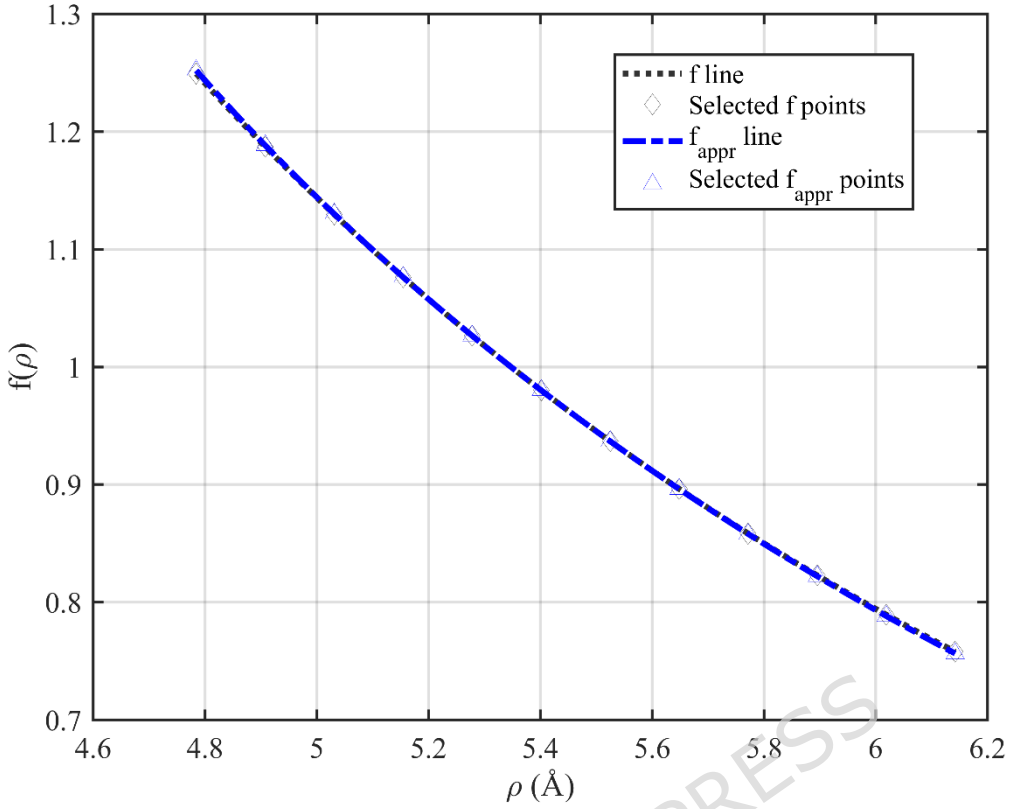

Figure 3: Comparison of the Pekeris-type approximation (g_{appr}) with the exact function (g) for the CO ($X\ ^1\Sigma^+$) molecule. The plot illustrates the fit of the approximation to the exact function

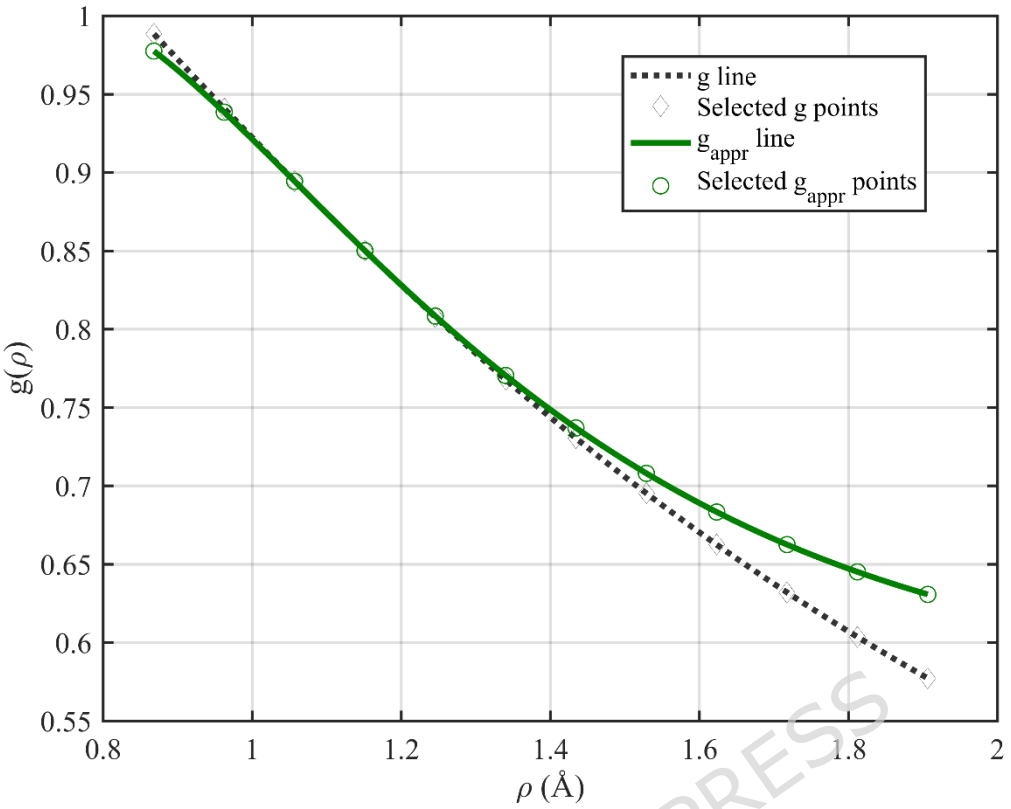

Figure 4: Comparison of the Pekeris-type approximation (g_{appr}) with the exact function (g) for the Cs_2 ($3\ ^3\Sigma_g^+$) molecule. The plot illustrates the fit of the approximation to the exact function

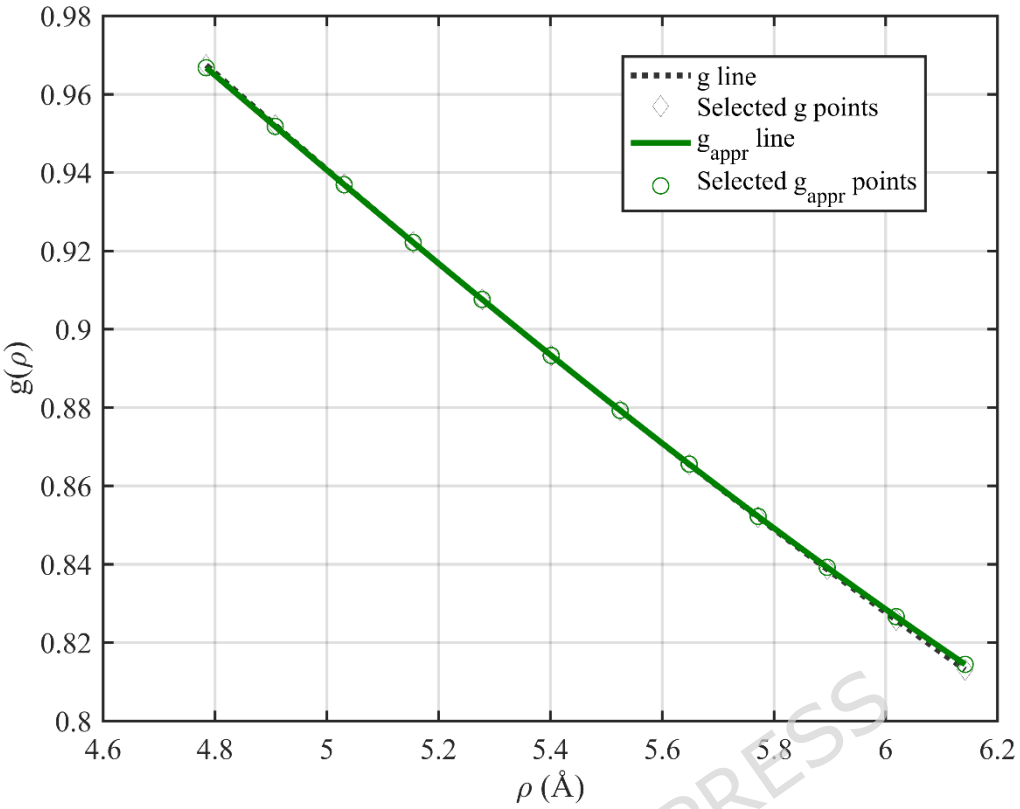

Figure 5: Temperature-dependent magnetization of Na_2 ($C(2)\ ^1\Pi_u$) dimer under external magnetic fields B = 50, 60, 70 T m^{-1} at $\Lambda_{AB} = 10^{-5}$ T Å